International Journal of Clinical and Health Psychology 23 (2023) 100342

International Journal of Clinical and Health Psychology

www.elsevier.es/ijchp

ORIGINAL ARTICLE

Effects of transcranial direct current stimulation on neural activity and functional connectivity during fear extinction

Dongha Lee[a,1,], Raquel Guiomar[b,1], Óscar F. Gonçalves[c], Jorge Almeida[c], Ana Ganho-Ávila[b,*]**

[a] *Cognitive Science Research Group, Korea Brain Research Institute, 61 Cheomdan-ro, Dong-gu, Daegu, Republic of Korea*
[b] *Center for Research in Neuropsychology and Cognitive Behavioral Intervention, Faculty of Psychology and Educational Sciences, University of Coimbra, Rua do Colégio Novo 3000-115, Coimbra, Portugal*
[c] *Proaction Laboratory, Center for Research in Neuropsychology and Cognitive Behavioral Intervention, Faculty of Psychology and Educational Sciences, University of Coimbra, Rua do Colégio Novo 3001-802 Coimbra, Portugal*

Received 30 March 2022; accepted 28 September 2022
Available online 15 October 2022

KEYWORDS
Fear extinction;
Resting-state functional connectivity;
tDCS;
Whole-brain searchlight classification

Abstract
Background/Objective: Anxiety disorders are highly prevalent and negatively impact daily functioning and quality of life. Transcranial direct current stimulation (tDCS) targeting the dorsolateral prefrontal cortex (dlPFC), especially in the right hemisphere impacts extinction learning; however, the underlying neural mechanisms are elusive. Therefore, we aimed to investigate the effects of cathodal tDCS stimulation to the right dlPFC on neural activity and connectivity patterns during delayed fear extinction in healthy participants. *Methods:* We conducted a two-day fear conditioning and extinction procedure. On the first day, we collected fear-related self-reports, clinical questionnaires, and skin conductance responses during fear acquisition. On the second day, participants in the tDCS group (n = 16) received 20-min offline tDCS before fMRI and then completed the fear extinction session during fMRI. Participants in the control group (n = 18) skipped tDCS and directly underwent fMRI to complete the fear extinction procedure. Whole-brain searchlight classification and resting-state functional connectivity analyses were performed. *Results:* Whole-brain searchlight classification during fear extinction showed higher classification accuracy of threat and safe cues in the left anterior dorsal and ventral insulae and

Abbreviations: CS, conditioned stimulus; dlPFC, dorsolateral prefrontal cortex; dAI, dorsal anterior insula; EPI, echo-planar imaging; FOV, field of view; fMRI, functional magnetic resonance imaging; GLM, general linear model; HC, hippocampus; IPL, inferior parietal lobule; PFC, prefrontal cortex; SCR, skin conductance response; tDCS, transcranial direct current stimulation; TE, echo time; TR, repetition time; US, unconditioned stimulus; vAI, ventral anterior insula; vmPFC, ventromedial prefrontal cortex; ACC, anterior cingulate cortex.

* Corresponding author at: Faculty of Psychology and Educational Sciences, University of Coimbra, 3000-115 Coimbra, Portugal.
** Corresponding author at: Cognitive Science Research Group, Korea Brain Research Institute, 61 Cheomdan-ro, Dong-gu, Daegu, Republic of Korea 41062.
E-mail addresses: donghalee@kbri.re.kr (D. Lee), ganhoavila@fpce.uc.pt (A. Ganho-Ávila).
[1] These authors contributed equally to the manuscript and should be considered as first authors.

https://doi.org/10.1016/j.ijchp.2022.100342

hippocampus in the tDCS group than in the control group. Functional connectivity derived from the insula with the dlPFC, ventromedial prefrontal cortex, and inferior parietal lobule was increased after tDCS. *Conclusion:* tDCS over the right dlPFC may function as a primer for information exchange among distally connected areas, thereby increasing stimulus discrimination. The current study did not include a sham group, and one participant of the control group was not randomized. Therefore, to address potential allocation bias, findings should be confirmed in the future with a fully randomized and sham controlled study.

Introduction

Anxiety disorders are highly prevalent and negatively impact the quality of life. Fear conditioning and extinction procedures are widely employed to model the therapeutic benefits of exposure-based therapies in ameliorating anxiety-related symptoms (Eysenck, 1979; Pitman & Orr, 1986). A recent meta-analysis (Foa & McLean, 2016) demonstrated that exposure-based therapies are moderately efficacious for anxiety disorders. However, more effective treatments are needed to increase extinction efficacy and address relapse which is common after treatment cessation (Bradley et al., 2005).

During fear conditioning, fear responses are acquired via repetitive pairing of conditioned (CS+) and aversive unconditioned (US) stimulus (Sotres-Bayon et al., 2006). Fear conditioning protocols involve the presentation of two stimuli: one that is predictive of the US (CS+) and another that is not predictive of the US (CS−) (LeDoux & Phelps, 2008). During fear extinction, the CS+ is presented repeatedly in the absence of US, leading to reduced fear expression (Lonsdorf et al., 2017; Phelps et al., 2004).

Functional magnetic resonance imaging (fMRI) studies of fear conditioning and extinction have characterized regions constituting the fear network. Exposure to a conditioned fear stimulus increases the activation of fear-processing regions, such as the amygdala, insula, and cingulate cortex (Hauner et al., 2012; Sevenster et al., 2018). Conversely, successful fear extinction is associated with decreased amygdala activation and reduced behavioral/physiological fear responses (Repa et al., 2001). Two approaches have been proposed for neural mechanisms underlying fear extinction; the top-down approach involves amygdala regulation by prefrontal cortex (PFC) control (Sotres-Bayon et al., 2006), and the bottom-up approach suggests that fear extinction occurs via changes in sensory processing of the CS+ (LeDoux & Phelps, 2008). In support of top-down mechanisms, PFC activity increases during extinction learning (e.g., Diekhof et al., 2011; Fullana et al., 2018; Milad et al., 2007; Phelps et al., 2004; Quirk & Mueller, 2008). Conversely, in support of bottom-up mechanisms, subcortical structures traditionally associated with fear learning (e.g., amygdala, hippocampus [HC], brainstem, and cerebellum) are recruited during extinction (e.g., Frontera et al., 2020; Herry et al., 2010).

Overlap between brain regions comprising the fear network in healthy individuals and brain regions associated with symptom severity in patients with anxiety suggests that targeting fear network regions using brain stimulation is clinically beneficial (Marin et al., 2014). Specifically, the PFC has been investigated for its role in decreasing the expression of previously acquired fear via top-down control of subcortical structures (Gilmartin et al., 2014). Accordingly, interventions that enhance PFC activity during fear extinction have received growing interest in the past (for a review, see (Fitzgerald et al., 2014)).

More recently, transcranial direct current stimulation (tDCS) targeting the dlPFC to modulate fear extinction has emerged as topical research in the field (Abend et al., 2016; Dittert et al., 2018; Nitsche & Paulus, 2000; van 't Wout et al., 2016). tDCS is a non-invasive brain stimulation method that alters cortical excitability by delivering a weak direct electric current to the brain (Nitsche & Paulus, 2000). The effects of tDCS on cognitive functions involved in fear extinction in healthy participants have been investigated using fear conditioning paradigms. For instance, Dittert et al. (Dittert et al., 2018) applied tDCS to the ventromedial prefrontal cortex (vmPFC) before and during fear extinction and observed that skin conductance responses (SCRs) decreased at the early phase of extinction for both stimuli, and lead to a generalization of the fear response to the CS− at the late phase of extinction. Similarly, van 't Wout et al. (2016) assessed the effect of anodal tDCS over the anterior PFC (anode over AF3; cathode over contralateral mastoid) and found that tDCS delivered during early extinction decreases SCR towards the CS+. The authors do not discuss what seems to be a generalization of the fear response to the CS− in late extinction. Abend et al. (2016) positioned the anode centrally over the forehead (cathode under the occipital bone) and delivering tDCS during fear extinction observed increased SCR response to the CS−, corresponding to a generalization of the fear response. The same authors, observed an impaired extinction learning when using alternating current. Ganho-Ávila et al. (2019) tested the effect of tDCS (cathode over rdlPFC, anode over left deltoid muscle) in a 3-day fear conditioning and extinction paradigm and found an impaired extinction learning, but a long-term positive tDCS effect on extinction learning with a decreased generalization effect to the CS− according to an approach-avoidance task, which, however, was not confirmed by SCRs.

Furthermore, some studies have investigated tDCS-driven modulation of cognitive and emotional processes relevant to anxiety. For instance, Ironside et al. (2019) tested whether stimulation over the PFC reduces amygdala threat reactivity during an attentional control task in healthy individuals with trait anxiety. The tDCS montage was bipolar balanced, with the anode over the ldlPFC and the cathode over the rdlPFC. Results showed that tDCS significantly reduced bilateral amygdalar reactivity to threat, with a simultaneously increased cortical activity in regions associated with attentional control. Vanderhasselt et al. (2017) examined the impact of tDCS on cognitive cost

applying tDCS over the rdlPFC (anode: F4, cathode: contralateral supraorbital area) and showed that tDCS enhanced cognitive control for emotional information in participants scoring high in rumination trait. Clarke et al. (2020) studied the impact of anodal tDCS over F3 (cathode over left superior trapezius muscle) on cognitive and emotional effects of worry and showed significantly increased state anxiety after instructed worry in the tDCS group compared to the sham group. The tDCS group also showed faster recovery and reductions in worry once the cognitive goals shifted to a non-worry focus. These studies suggest the beneficial effect of tDCS over the rdlPFC in boosting fear extinction-related processes, such as stimuli discrimination, vigilance, cognitive control, and attention.

There is increasing research about the clinical applications of tDCS in clinical samples (for a review, see (Stein et al., 2020). The beneficial effects of tDCS on anxiety symptoms when the cathode is placed over the rdlPFC are of particular interest (Sadeghi Movahed et al., 2018; Shiozawa et al., 2014). Overall, these studies demonstrated the importance of electrode polarity at the targeted region, and the inconsistency across studies for methodological parameters, targeted processes, and results. These promising results inspired Ganho-Ávila et al (2019) paper where we showed that tDCS over the rDLPFC (cathode: rDLFC; anode: left deltoid muscle) before fear extinction did not improve fear learning, as measured by SCR, but it eliminated the overgeneralization of the fear response to the CS− observed in the sham group (an effect of tDCS previously reported by other authors after anodal tDCS over the vmPFC, e.g. (Abend et al., 2016; Dittert et al., 2018)). Further, in our previous publication (Ganho-Ávila et al., 2022) we showed that cathodal tDCS over the rDLPFC boosted the connectivity between regions of the prefrontal cortical−amygdalo−hippocampal−cerebellar fear pathway during subsequent extinction training. However, in Ganho-Ávila et al., 2022, our early vs. late extinction analysis might have hindered the variability across the extinction session, that a trial-by-trial approach can offer. Additionally, recent studies have employed multivariate fMRI pattern analysis to clarify the neural mechanics associated with fear conditioning and expression while accounting for inter-subject variability and complex multi-voxel patterns (Graner et al., 2020; Sjouwerman et al., 2020; Whitehead & Armony, 2019; Zhou et al., 2021).

Considering these recent findings and methodological approaches, in the current study we aim to expand our previous results and clarify the impact of cathodal tDCS applied to rDLPFC in whole-brain discrimination accuracy between CS+ and CS− on a trial-by-trial approach. We hypothesize that fear discriminability (the ability to discriminate between CS+ and CS−) will be decreased in fear-processing brain regions after cathodal tDCS to the rDLPFC, thus indicating successful extinction learning. As a secondary aim, we will conduct an exploratory resting-state connectivity analysis to test the impact of tDCS on a set of regions of interest that show significant between-group differences in classification accuracy. Informed by previous results (Ganho-Ávila et al., 2022), we expect that tDCS will boost connectivity among subcortical structures (e.g. hippocampus, insula, cerebellum), and between those and the contralateral cortical regions (e.g. left DLPFC, left VMPFC).

Materials and methods

This study is a re-analysis of the functional data collected in (Ganho-Ávila et al., 2022), complemented with the analysis of resting-state data. The sample size calculation was originally estimated for the analysis reported on Ganho-Ávila and colleagues' study (Ganho-Avila et al., 2022).

Participants

Participants were recruited via social media posts and advertisements at the University. In total, 48 women were included, providing written informed consent. The study was approved by the ethics committee of the [Faculty of Psychology and Educational Sciences, University of Coimbra]. Participants received a voucher of €30 upon completing participation. The exclusion criteria were (1) a history of psychiatric disorders; (2) use of psychoactive medication; (3) pregnancy; (4) caffeine and/or alcohol intake 24 h before sessions; (5) physical exercise 2 h before sessions; (6) consuming a meal 2 h before sessions (Boucsein et al., 2012); (7) auditory or visual (non-corrected) deficits; and (8) standard exclusion criteria for MRI scanners. Based on previous literature (Agren et al., 2012; LaBar et al., 1998; Phelps et al., 2004) and the aposteriori sample size estimation for whole-brain searchlight classification analysis (for α = .001, power .90, an effect size of .30, and 10% dropouts), a minimum of 13 participants per group was established.

Procedure (AB design)

Participants completed a partial auditory fear conditioning procedure (75% reinforcement rate) for 2 consecutive days for fear memory consolidation. Prior to commencing experiments, participants underwent brief assessment for exclusion criteria and collection of baseline demographic and clinical data (general psychopathology, anxiety state, trait, and sensitivity). On day 1, the fear conditioning procedure occurred in context A (university laboratory), and SCRs, self-report ratings of valence, arousal contingency, and expectancy were collected. On day 2, the tDCS group received an active 20-minute, 1 mA tDCS session (cathode over F4 and anode over left deltoid muscle), and then completed the fear extinction session. The control group skipped the tDCS session and started day 2 with the fear extinction task. The fear extinction procedure occurred in context B (fMRI scanner), and functional MRI data were collected. E-Prime (2.0.10.353 Standard SP1, Psychology Software Tools, Pittsburgh, PA) was used to script the experiments and collect data (See Fig. 1). Tasks were presented over a white background using a DELL P2012H monitor. US triggers and onset markers were processed using a second computer, which collected electrodermal activity across habituation and acquisition sessions. The extinction session occurred on day 2 inside the fMRI scanner, in which stimuli were presented on an Avotec projector, controlled by "A Simple Framework (Schwarzbach, 2011)" in MATLAB R2014a (The MathWorks Inc., Natick, MA, USA) using an in-house script. Stimuli were presented via a mirror attached to a head coil.

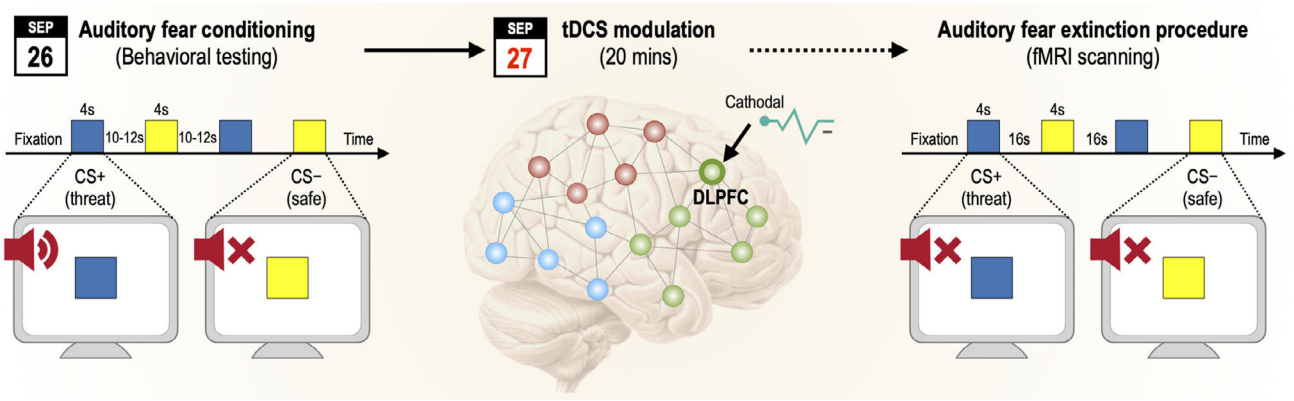

Fig. 1 Overview of the experimental procedure for fear conditioning and extinction.

Experimental stimuli

Three stimuli were presented—US, CS+, and CS− (never paired with the US). The US was a woman's scream (item 277 of the International Affective Digitized Sound System) (Yang et al., 2018). The US volume intensity was individually set to an uncomfortable but non-painful intensity (90–96 dB) with a dummy aversive sound according to the visual analog scale for pain ratings (Huskisson, 1974). Auditory stimuli were presented via noise-cancelling headphones. Colored squares (blue and yellow) were randomly assigned and counterbalanced across participants as CS+ or CS−. The CSs and US were presented for 4 s and 2 s, respectively, with the latter overlapping the last 2 s of the CS+ presentation. The CS presentation order was pseudorandomized such that no more than two consecutive presentations of the same stimulus occurred.

Day 1: Habituation and fear acquisition (context A)
The habituation phase comprised eight non-reinforced CS+ and eight CS− presentations. The acquisition phase comprised a partial reinforcement procedure at 75% (12 of 16 CS + presentations were paired with the US). In total, 16 CS+ and 16 CS− trials were presented. In both the habituation and acquisition phases, each stimulus was presented for 4 s over a white screen, followed by a jittered inter-stimulus interval between 10 and 12 s, during which a black fixation cross was presented at the center of the screen. On day 1, only participants who acquired the fear response were invited to participate on day 2 (24 h later). Successful fear acquisition was defined as a positive SCR differential in the last five trials (CS+ > CS−). If habituation to the US occurred, the middle phase (from the 6th to 10th trial inclusive) was considered. The minimum difference of 0.01 μS between CS+ and CS− was assumed (Oyarzun et al., 2012).

Day 2: tDCS session and fear extinction (context B – MRI scanner)
On day 2, participants underwent tDCS before fMRI or underwent fMRI alone. tDCS (1 mA for 20 min) was delivered via a one-channel stimulator (TCT Research Limited, Hong Kong). The cathode was placed over the rdlPFC (F4, 10/20 international system (Klem et al., 1999)). The anode was placed over the contralateral deltoid muscle (extra-cephalic montage). Sponges of 5 cm^2 were saturated with 10 mL 0.9% saline solution. Participants were instructed to remain still and calm during tDCS. Offline tDCS was preferred over online tDCS to prevent MRI artifacts due to electrical current (Antal et al., 2014). After the tDCS session, adverse effects were assessed according to Thair (2017). Before entering the scanner, participants were instructed to recollect the color of the square associated with the US on the previous day. No further information was provided regarding the auditory stimuli. The session comprised 10 CS+ and 10 CS− trials. Each trial involved the presentation of a fixation cross for 16 s followed by the presentation of the CS+ or CS− for 4 s. The US had not been previously presented. Participants viewed the images passively for 7 min according to a block design.

Data acquisition and preprocessing

All MRI data were collected using a Siemens Tim Trio 3-T MRI scanner (Erlangen, Germany) with a 12-channel head coil. High-resolution T1-weighted image data were obtained using a magnetization-prepared rapid acquisition gradient echo pulse sequence with the following parameters: repetition time (TR) = 2530 ms, echo time (TE) = 3.29 ms, flip angle = 7°, field of view (FOV) = 256 × 256 mm, acquisition matrix size = 256 × 256, voxel size = 1.0 × 1.0 × 1.0 mm^3, and number of slices = 192. fMRI data for resting state and fear extinction were acquired using a T2*-weighted single-shot echo-planar imaging (EPI) sequence with the following parameters: TR = 2000 ms, TE = 30 ms, flip angle = 90°, FOV = 256 × 256 mm, acquisition matrix size = 64 × 64; voxel size = 4.0 × 4.0 × 4.0 mm^3, number of slices = 30 (interleaved), and number of scans = 180 for resting state and 210 for fear extinction.

All fMRI data were preprocessed using SPM12 (http://www.fil.ion.ucl.ac.uk/spm, Wellcome Trust Centre for Neuroimaging, London, UK) (Friston et al., 1995). All fMRI data underwent standard preprocessing steps, including slice timing (for scan time correction), realignment (for head motion correction), co-registration of T1-weighted image, and spatial normalization of functional data into Montreal Neurological Institute space using nonlinear transformation in SPM12. Normalized functional data were interpolated to 2.0 × 2.0 × 2.0 mm^3 voxels. To avoid spillover effects between voxels, spatial smoothing was not conducted (Haxby et al., 2001; Haynes & Rees, 2006; Norman et al., 2006; Todd et al., 2013).

Whole-brain searchlight classification

To estimate neural activity during CS+ and CS− stimulus, we used a general linear model (GLM) where observed signal *Y* at a voxel *i* is represented by a linear combination of a design matrix *X* and its weight vector β and noise ε. The GLM model was defined as below.

$$Y_i = \beta_1 X_{i1} + \beta_2 X_{i2} + \varepsilon_i, \varepsilon_i \sim N(0, \sigma^2).$$

Beta values (or regression coefficients, β) for CS+ and CS− were estimated by applying the GLM with regressors convolved with a canonical hemodynamic response. To evaluate the effect of tDCS on fear extinction, support vector machine (SVM) classification of fMRI data in each individual was performed using a whole-brain searchlight approach (Kriegeskorte et al., 2006). A spherical searchlight (6 mm radius) comprising 123 voxels was created. At every voxel, the β-values per condition were vectorized to create a pattern, and 20 patterns (10 trials $\times$ 2 classes) were extracted. A SVM with 5-fold cross-validation was used for the classification (Boser et al., 1992; Cortes & Vapnik, 1995). A linear SVM classifier was trained using the patterns (16 samples, 2 classes $\times$ 8 trials) with hyperparameter C = 1 (Andersson et al., 2013; Lee et al., 2019; Sitaram et al., 2011) and tested with the remaining patterns (4 samples $\times$ 2 classes). The mean classification accuracy after 5-fold cross-validation was assigned to the central voxel.

To assess the statistical significance of the mean classification accuracy, one-sample t-tests were conducted after subtracting 0.5 (chance level) from the mean accuracy at each voxel. Group differences in the classification accuracy maps were computed using two-sample t-tests. Extraction of significant voxels was performed as reported previously (Chen et al., 2016). For the group-level inference, a voxel-level threshold of $p < 0.05$ was set, with an extent threshold of 38 and 63 voxels per cluster for the tDCS and control groups, respectively. Further, cluster-level threshold of $p < 0.05$ was used to correct for multiple comparisons using 10,000 Monte Carlo simulations (Scholz et al., 2009; Xiong et al., 1995) with REST's AlphaSim (http://restfmri.net) (Ward, 2000). For group comparisons, clusters comprising a minimum of 40 voxels with a threshold of $p < 0.05$ corrected by the cluster size threshold as described above.

Resting-state functional connectivity

Considering signal stability, the first five images of resting-state fMRI were discarded. The remaining 205 EPI images were preprocessed using standard procedures with SPM12. All fMRI time series were estimated by regressing out six rigid motions and their derivatives, three principal components of white matter and cerebrospinal fluid masks, linear repressors, quadratic regressions, and high-pass filtering with a cutoff frequency of 0.009 Hz.

Peak coordinates of the left dorsal anterior insula (dAI), ventral anterior insula (vAI), and HC were used as seed ROIs, given the involvement of these regions to discriminate between CS+ and CS− processing (dAI: −30, 14, −18; vAI: −46, 6, −2; HC: −24, −16, −20). Whole-brain resting-state functional connectivity was calculated with correlation coefficients between the average time series of the searchlight (123 voxels) derived from the peak coordinates and those of whole-brain voxels. The correlation coefficients were transformed into Fisher's z-values. Functional connectivity maps were obtained for each participant. Group differences in functional connectivity maps were analyzed using two-sample t-tests for each voxel. Clusters comprised a minimum of 100 voxels with a false discovery rate threshold of $p < 0.01$. For group comparisons, clusters comprised a minimum of 85, 71, and 72 voxels for dAI, dVI, and HC, respectively, with a threshold of $p < 0.05$. corrected for multiple comparisons by cluster-level threshold estimated using 10,000 Monte Carlo simulations.

Statistical analysis of classification accuracy and anxiety-related scores

Anxiety-related scores of state and trait anxiety were measured using the STAI (STAI-1 and STAI-2, respectively (Spielberger, 1983)). The associations between state and trait anxiety before fear conditioning (day 1) and classification accuracy calculated in the left dAI, dVI, and HC during fear extinction (day 2) were analyzed using Pearson correlation analysis.

Results

Three participants withdrew due to discomfort during the experimental task, eight were excluded due to unsuccessful fear acquisition on day 1, and data from three participants were not recorded due to technical issues. Finally, data from 34 women were analyzed (all of whom successfully acquired the fear response on day 1). Participants were assigned to the tDCS (n = 16, mean age = 24.19 years, standard deviation [SD] = 5.94 years) and control (n = 18, mean age = 22.56 years, SD = 5.47 years) groups by random when no excluding criteria were present. As per informed consent, when excluding criteria were present, or participants were not willing to receive tDCS, they were allocated to the control group. Seventeen participants were randomly allocated to the control group, one was allocated due to the presence of tDCS exclusion criteria, and zero due to unwillingness to receive tDCS. No significant between-group baseline differences in anxiety state, trait, sensitivity, and general psychopathology were observed (p = .71, p = .60, p = .28, and p = .97, respectively).

Classification accuracy differences

One-sample t-tests comparing the mean accuracy at each voxel with zero (after subtracting the chance level) showed increased discrimination between the CS+ and CS− in the left HC, superior/middle occipital gyrus, cerebellum, and vermis regions, in the tDCS group; and in the left superior occipital gyrus and calcarine in the control group. Two-samples t-test revealed that classification accuracy in the left dAI, left vAI, and HC was significantly higher in the tDCS group than in the control group, whereas that in the left middle frontal gyrus, middle cingulum, right superior frontal gyrus, and middle temporal gyrus was significantly higher in the control group than in the tDCS group (Fig. 2; Table 1).

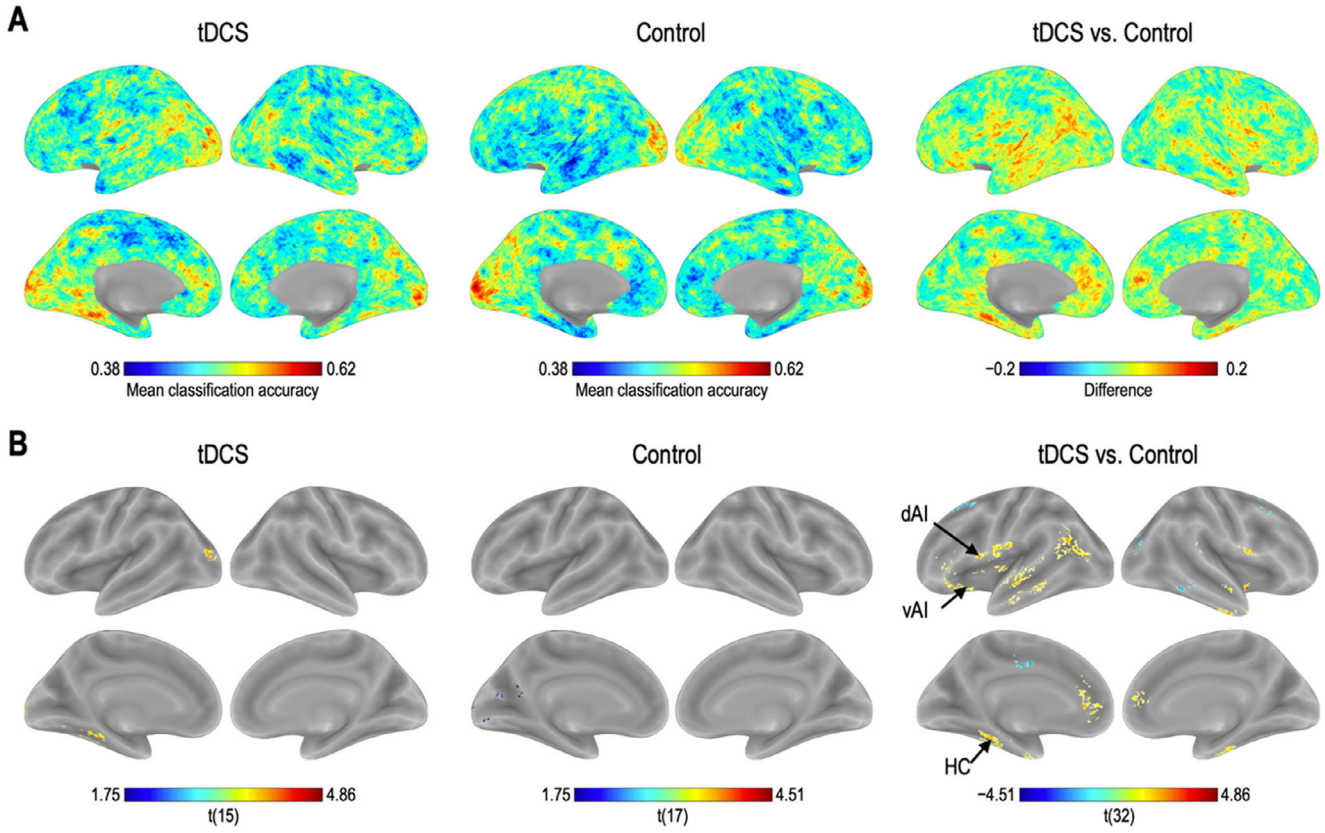

Fig. 2 Whole-brain searchlight classification accuracy results (A). Compared to the control group, the tDCS group exhibited significantly increased classification accuracy in the left dorsal anterior insula (dAI), left ventral anterior insula (vAI), and hippocampus (HC) (B).

Functional connectivity differences

Functional connectivity of the left vAI with the left HC, right vmPFC, parahippocampus, and dlPFC was significantly greater in the tDCS group than in the control group (Fig. 3A; Table 2). Functional connectivity of the left dAI with the left HC and right dlPFC was significantly greater in the tDCS group than in the control group (Fig. 3B; Table 3). The left HC exhibited increased functional connectivity with the left vAI and bilateral vmPFC in the tDCS group compared to the control group (Fig. 3C; Table 4).

Relationship between classification accuracy and anxiety-related measures

The STAI-2 scores and classification accuracy in the left vAI were positively correlated in the tDCS group (r = 0.46, p = 0.0374) but not in the control group (r = 0.11, p = 0.3325) (Fig. 4). However, after exclusion of an outlier value in the tDCS group, correlation results were not significant (r = 0.40, p = 0.0720). No correlation was observed between the STAI-2 scores and classification accuracy in the left dAI in the tDCS (r = 0.09, p = 0.3634) and control (r = −0.27, p = 0.1394) groups. Similarly, no correlation was observed between the STAI-2 scores and classification accuracy in the HC in the tDCS (r = −0.24, p = 0.1858) and control (r = 0.37, p = 0.0670) groups, and no correlations were found between STAI-1 and classification accuracy across brain areas and groups.

Discussion

We reported the effects of cathodal tDCS stimulation to the right dlPFC on neural activity during fear extinction and resting-state functional connectivity after extinction learning.

By performing MVPA (Haxby et al., 2001; Kamitani & Tong, 2005; Norman et al., 2006; Pereira et al., 2009) with searchlight methods (Kriegeskorte et al., 2006), we showed whole-brain information-mapping during fear extinction after cathodal tDCS stimulation over the rdlPFC and no stimulation. Based on our previous study (Ganho-Avila et al., 2019), it was expected that the discriminability of CS+ (threat cues) and CS− (safe cues) processing would be differed between groups. Indeed, participants in the tDCS group exhibited increased fear discriminability in the dAI, vAI, and HC, suggesting that the cathodal tDCS stimulation to the rdlPFC can modulate neural patterns in fear-related brain regions that are distally connected to the rdlPFC. For example, cathodal tDCS stimulation affected the transfer of fear-related information and indirectly modulated the extent to which fear information is spatially encoded across voxels within the left insular cortex (dorsal and ventral). These results are consistent with those of previous reports on the critical role of the insular cortex in fear extinction (Dunsmoor et al., 2019; Fullana et al., 2018; Fullana et al., 2016) and with reports of distal alterations in neural activity patterns and functional connectivity (Lee et al., 2019). Moreover, tDCS stimulation operated as a primer for information exchange regarding fear extinction between distally

Table 1 Brain regions showing statistically significant differences in classification accuracies during fear extinction. L: left, R: right.

Regions (AAL abbreviation)	MNI coordinates			Clustersize (mm^3)	t−value
	x	y	z		
tDCS group					
Lobule VI of cerebellar hemisphere L	−20	−66	−20	680	4.84
Lobules IV, V of cerebellar hemisphere L	−22	−46	−20	1208	4.31
Middle occipital gyrus L	−30	−92	16	512	4.13
Lobule IV, V of vermis L	2	−52	−14	528	3.56
Superior occipital gyrus L	−12	−100	8	368	3.47
Hippocampus L	−32	−30	−12	1208	3.61
Control group					
Calcarine L	−4	−92	−4	904	3.86
Calcarine L	−10	−60	8	560	3.66
Calcarine L	−12	−76	8	904	2.19
Superior occipital gyrus L	−12	−98	18	904	2.17
tDCS group > control group					
Inferior frontal gyrus (triangular part) L	−44	38	12	744	5.55
Lobule VI of cerebellar hemisphere L	−14	−68	−24	1000	5.26
Temporal pole (middle temporal gyrus) R	40	14	−34	872	4.95
Insula L (ventral anterior)	−30	14	−18	1176	4.86
ParaHippocampal gyrus L	−30	−36	−14	2464	4.44
Fusiform gyrus R	36	−24	−26	1984	4.42
Insula L (dorsal anterior)	−46	6	−2	952	3.96
IFG pars orbitalis L	−46	26	−4	1176	3.95
Inferior temporal gyrus R	48	−10	−38	1984	3.80
Middle temporal gyrus L	−50	−18	−10	1152	3.78
Superior anterior cingulate cortex L	−6	36	6	720	3.75
Rolandic operculum R	58	2	8	528	3.75
Anterior cingulate cortex (pregenual) R	14	44	10	440	3.70
Rolandic operculum L	−48	−10	12	2584	3.63
Inferior temporal gyrus L	−66	−32	−18	408	3.47
Middle temporal gyrus L	−46	−58	20	1512	3.46
Inferior temporal gyrus L	−64	−14	−26	1152	3.40
Inferior temporal gyrus L	−40	−14	−36	504	3.35
Lobule VI of cerebellar hemisphere R	26	−58	−22	920	3.28
SupraMarginal gyrus R	66	−34	26	520	3.27
Superior temporal gyrus R	62	−4	−10	344	3.15
Lobule IV, V of vermis	6	−52	−14	920	3.13
Anterior cingulate cortex (supracallosal) L	−10	30	28	720	2.83
Superior temporal gyrus L	−56	−2	−8	2584	2.80
Postcentral gyrus L	−62	−22	22	2584	2.76
Middle temporal gyrus L	−64	−38	4	1152	2.66
Middle occipital gyrus L	−44	−78	16	1512	2.66
Inferior temporal gyrus L	−44	−26	−26	2464	2.23
Hippocampus L	−24	−16	−20	2464	1.89
tDCS group < control group					
Lobule IX of cerebellar hemisphere L	−16	−40	−46	488	5.138
Inferior temporal gyrus R	60	−52	−16	376	4.879
Superior occipital gyrus R	28	−80	18	408	3.857
Middle cingulate gyrus L	−6	−10	42	456	3.837
Calcarine L	4	−86	8	400	3.469
Middle frontal gyrus L	−26	28	44	712	3.396
Crus II of cerebellar hemisphere R	46	−70	−42	352	3.176
Superior frontal gyrus (dorsolateral) R	28	12	52	408	3.053

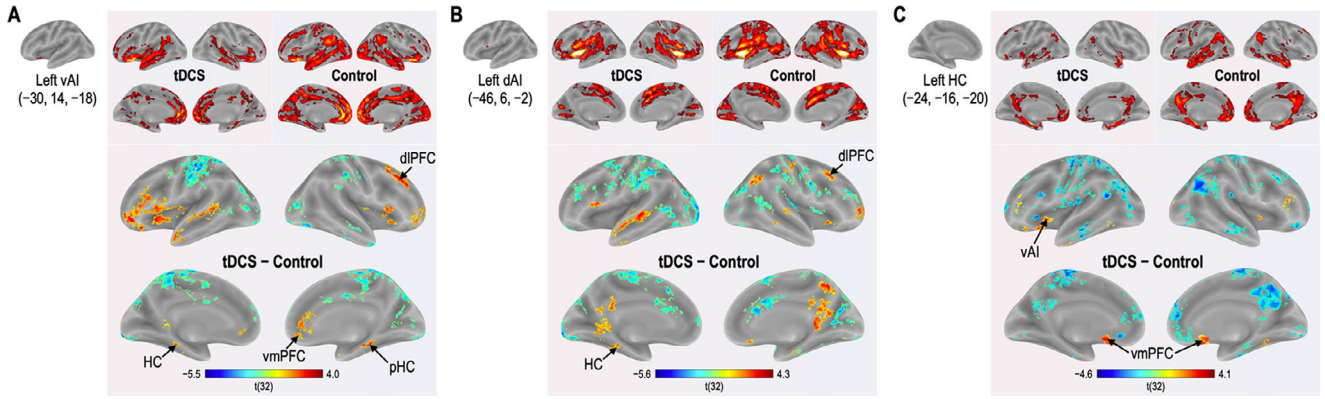

Fig. 3 Functional connectivity differences derived from the left vAI (A), dAI (B), and HC (C). Compared to the control group, the tDCS group exhibited increased functional connectivity among fear-related brain regions (the left vAI, dAI, HC, vmPFC, and dlPFC).

connected areas increasing discriminability between CSs. Particularly, group comparison results suggest that tDCS had an effect on other regions involved both in fear expression and regulation across both hemispheres such as lobule IV of the cerebellum, cerebellar vermis, left and right ACC, left and right rolandic operculum, left HC, left parahippocampal gyrus, and left postcentral gyrus. Of particular interest, tDCS was found to modulate left ventral and dorsal AI, and left HC accuracy besides cortical regions, contrary to the control group. This suggests that tDCS might have a particular effect in bottom-up regulation of the fear response.

Based on previous experimental studies (Ganho-Avila et al., 2019) and clinical case reports (Shiozawa et al., 2014) showing promising effects of placing the cathode over the rdlPFC (and anode over the left deltoid), we expected that this montage would boost fear extinction, and thus, lead to decreased classification accuracies across fear-related regions. However, contrary to our expectation, classification accuracies were increased after cathodal tDCS stimulation. Increased classification accuracies might be associated with the reflection of overgeneralization that has been previously reported across distinctive tDCS montages and electrode polarities (Abend et al., 2016; Ganho-Avila et al., 2019). Previous literature shows that overgeneralization of the fear response might be associated with both increased and decreased classification accuracies during fear extinction. For example, after extinction Abend et al. (2016), found an increased fear response to the CS+ (unsuccessful fear extinction), concomitant with an increased fear response to the CS− (overgeneralization of the fear response to the CS−) which led to a reduced classification accuracy between stimuli. However, Dittert et al. (2018) and ourselves (Ganho-Avila et al., 2022) found a decreased fear response to the CS + (successful extinction) concomitant with an increased fear response to the CS− (also considered an overgeneralization of the fear response to the CS−). Indeed, our earlier analysis of this same dataset showed two activation clusters (one including the frontal middle and the frontal superior left cortices, and another including the left and the right paracentral region and the right postcentral area) with this exact pattern in the tDCS group compared to the control group (Ganho-Avila et al., 2022). However, these two clusters do not directly overlap with the brain regions showing increased accuracies in the current study. This might be due to the different analytic approaches. While in Ganho-Ávila et al. (2022) analysis were conducted over averaged brain activation comparing early vs late extinction, in the current study we observed brain activation on a trial-by-trial bases. Future studies should further explore the possible distinct mechanisms underlying overgeneralization of the fear response to the CS− and its translational meaning, thus clarify the results of the current paper.

The study by Graner et al. (2020) tested the neural representation across the brain with a MVPA approach during fear extinction, where higher dissimilarity between voxels activity in one same region during the processing of a stimulus across time would indicate lower stability of the stimulus representation, and consequently better fear extinction. The authors found that clusters centered at the right and left rolandic operculum, cerebellum, mid-cingulate cortex, and postcentral gyrus, showed increased dissimilarity, meaning successful extinction learning. Graner et al.'s findings are in contrast with our results, where tDCS seems to have impaired fear extinction, as the same regions showed increased accuracies between CSs.

To further test the effects of cathodal tDCS stimulation in functional connectivity after fear extinction learning, we evaluated resting-state functional connectivity maps using our principal findings that fear discriminability in the left insular cortex (dorsal and ventral anterior) and hippocampus was affected by cathodal tDCS stimulation. Functional connectivity between the left insular cortex (dorsal and ventral anterior) and bilateral dlPFC was greater in the tDCS group once more supporting tDCS−driven modulatory changes in functional connectivity patterns between distally connected regions. These results agree with previous findings indicating global integration of information via long-range connections (Bullmore & Sporns, 2009; Deco et al., 2011; Deco et al., 2015; Friston, 2011; Park & Friston, 2013). The fMRI evidence for functional connections among distributed brain regions in fear processing is growing. Our study contributes to the field by showing that tDCS with the cathode over the right dlPFC (and anode over contralateral deltoid muscle) changes the connectivity patterns between distal subcortical regions within the prefrontal cortical−amygdalo−hippocampal−cerebellar pathway. Particularly, our results indicated that the left insular cortex exhibited greater connectivity with the bilateral dlPFC and left vmPFC after cathodal tDCS. Our study is in line with

Table 2 Functional connectivity maps from the left ventral anterior insula in tDCS and control groups. L: left, R: right.

Regions (AAL abbreviation)	MNI coordinates			Clustersize (mm^2)	t−value
	x	y	z		
tDCS group > control group					
Inferior frontal gyrus (triangular part) L	−32	30	−12	95776	3.865
IFG pars orbitalis L	−4	0	10	95776	3.842
Parahippocampal gyrus R	22	−52	−20	5408	2.268
Lobule IV, V of cerebellar hemisphere R	−48	0	−24	1912	3.683
Middle temporal gyrus L	30	28	36	3888	3.557
Middle frontal gyrus R	24	16	52	3888	2.938
Superior frontal gyrus (dorsolateral) R	22	54	−2	3744	3.329
Superior frontal gyrus (dorsolateral) R	50	46	−10	3744	2.651
IFG pars orbitalis R	4	40	−8	2768	3.314
Superior frontal gyrus (medial orbital) R	8	34	16	2768	2.995
Anterior cingulate cortex (supracallosal) R	50	16	4	696	3.128
Inferior frontal gyrus (opercular part) R	−16	−48	−16	2120	3.004
Lobule IV, V of cerebellar hemisphere L	−36	−42	−34	2120	2.766
Lobule VI of cerebellar hemisphere L	−18	−46	2	2336	2.938
Precuneus L	−24	−28	−10	2336	2.107
Hippocampus L	−56	−42	4	2312	2.916
Middle temporal gyrus L	−64	−22	2	2312	2.810
Middle temporal gyrus L	−48	−58	14	2312	2.294
Middle temporal gyrus L	36	−36	−24	776	2.839
Fusiform gyrus R	−16	−86	−30	66016	1.709
tDCS group < control group					
Crus II of cerebellar hemisphere L	42	−68	−20	66016	2.251
Fusiform gyrus R	−16	−88	−16	66016	5.530
Lingual gyrus L	50	−70	−18	66016	5.373
Fusiform gyrus R	4	−42	−24	66016	4.296
Lobule I, II of vermis	−52	−56	−26	66016	4.244
Crus I of cerebellar hemisphere L	22	−100	−10	66016	3.839
Lingual gyrus R	−40	−28	54	95776	5.197
Postcentral gyrus L	−32	−42	68	95776	4.661
Postcentral gyrus L	30	−88	34	95776	4.439
Middle occipital gyrus R	−10	−48	50	95776	4.325
Precuneus L	4	−52	64	95776	4.139
Precuneus R	−4	66	16	21736	4.812
Superior frontal gyrus (medial) L	8	32	60	21736	4.739
Superior frontal gyrus (medial) R	−26	56	32	21736	4.397
Middle frontal gyrus L	−8	48	50	21736	3.395
Superior frontal gyrus (medial) L	−2	68	−4	21736	3.392
Superior frontal gyrus (medial orbital) L	54	0	−42	2504	4.412
Inferior temporal gyrus R	34	0	−36	2504	2.379
Fusiform gyrus R	26	6	−28	1200	4.099
Parahippocampal gyrus R	64	−8	42	768	3.735
Postcentral gyrus R	42	−24	38	1776	3.599
Postcentral gyrus R	58	−38	34	1776	2.852
SupraMarginal gyrus R	−34	−76	30	6104	3.531
Middle occipital gyrus L	−40	−80	8	6104	3.365
Middle occipital gyrus L	54	−16	−20	2008	3.517
Inferior temporal gyrus R	42	−36	−16	2008	2.174
Fusiform gyrus R	−54	24	24	95776	4.040

previous research considering the insula as a hub for integrating visceral/sensory-related information, and communicating with regions responsible for top-down regulation, such as the dlPFC and vmPFC (Berntson et al., 2011; Gu et al., 2013). However, future studies should observe simultaneously collected self-reported measures of fear and SCR which would complement fMRI data and offer meaningful insights to classification accuracy.

Classification accuracy in the left vAI was positively correlated with trait anxiety (STAI-2) in the tDCS group but not in the control group. This suggests that for individuals who tend to be more anxious, tDCS might have contributed to

Table 3 Functional connectivity maps from the left dorsal anterior insula in tDCS and control groups. L: left, R: right.

Regions (AAL abbreviation)	MNI coordinates			Clustersize (mm^2)	t−value
	x	y	z		
tDCS group > control group					
Precuneus R	6	−58	46	1824	4.252
Superior frontal gyrus (dorsolateral) R	30	64	0	4320	3.665
Middle temporal gyrus R	72	−36	−6	3368	3.601
Middle temporal gyrus R	66	−10	−12	3368	2.272
Inferior parietal gyrus L	−34	−72	46	2744	3.600
Superior temporal gyrus L	−48	−6	−6	3328	3.590
Middle temporal gyrus L	−54	−32	0	3328	3.228
Lobule IV, V of cerebellar hemisphere L	−6	−50	0	2344	2.684
Inferior parietal gyrus R	52	−54	50	7360	3.483
Angular gyrus R	36	−68	54	7360	3.347
Superior parietal gyrus R	30	−54	72	7360	2.665
Angular gyrus R	50	−72	38	7360	2.417
Postcentral gyrus R	34	−26	48	808	3.471
Precuneus R	10	−50	26	4664	3.465
Calcarine L	0	−66	12	4664	3.350
Lobule IV, V of vermis	8	−46	2	4664	3.056
Posterior cingulate gyrus L	−10	−42	28	4664	2.382
Putamen R	26	−4	14	11904	3.362
Inferior temporal gyrus L	−44	−10	−36	624	3.338
Rectus L	−4	64	−16	1160	3.279
Lobule IX of cerebellar hemisphere L	−2	−52	−54	1544	3.263
Temporal pole (middle temporal gyrus) L	−54	14	−30	1128	3.258
Middle frontal gyrus R	42	26	50	1920	3.221
Rectus R	2	24	−16	952	3.186
Caudate L	−8	20	8	53160	3.146
Caudate L	−8	2	18	53160	2.640
SupraMarginal gyrus L	−60	−22	42	53160	1.929
tDCS group < control group					
Inferior frontal gyrus (triangular part) L	−50	16	8	1264	3.106
Middle temporal gyrus L	−66	−20	0	768	2.165
Crus II of cerebellar hemisphere L	−44	−58	−48	1008	2.886
Fusiform gyrus L	−34	−38	−18	688	2.689
Lingual gyrus L	−12	−90	−16	59704	1.913
Precentral gyrus R	56	2	36	4616	1.876
Inferior occipital gyrus L	−20	−100	−10	59704	5.587
Lobule VI of cerebellar hemisphere R	28	−52	−34	59704	4.676
Middle occipital gyrus L	−32	−80	20	59704	4.134
Superior occipital gyrusL	−20	−72	36	59704	3.946
Superior parietal gyrus L	−22	−62	56	53160	4.597
Anterior cingulate cortex (supracallosal) L	0	20	24	53160	4.463
Supplementary motor area L	0	12	44	53160	4.376
SupraMarginal gyrus L	−52	−30	30	53160	4.372
Supplementary motor area R	12	8	72	53160	4.109
Postcentral gyrus R	34	−36	50	3272	4.573
Postcentral gyrus R	32	−38	70	3272	3.299
Precentral gyrus R	52	8	38	4616	4.119
Middle frontal gyrus R	42	−4	52	4616	3.108
Postcentral gyrus R	68	−10	28	4616	3.067
Precentral gyrus R	62	8	20	4616	1.807
Middle occipital gyrus L	−40	−80	8	6944	4.024
Middle temporal gyrus L	−52	−58	6	6944	3.790
Crus I of cerebellar hemisphere L	−52	−56	−26	6944	3.274
Inferior occipital gyrus L	−40	−68	−10	6944	3.009
Postcentral gyrus R	52	−22	38	1096	3.999
Heschl's gyrus R	36	−32	14	1832	3.843
Red nucleus R	6	−16	−10	11904	3.731

Table 3 (*Continued*)

Regions (AAL abbreviation)	MNI coordinates			Clustersize (mm^2)	t−value
	x	y	z		
Middle frontal gyrus L	−32	38	16	5408	3.630
Middle frontal gyrus L	−42	40	36	5408	2.759
Middle frontal gyrus L	−30	18	32	5408	2.316
Middle temporal gyrus R	50	−52	14	4176	3.374
Middle temporal gyrus R	50	−38	−2	4176	2.054
Middle frontal gyrus R	38	34	22	2864	3.370
Middle frontal gyrus R	34	42	42	2864	3.277
SupraMarginal gyrus R	70	−22	24	1424	3.235
SupraMarginal gyrus R	52	−34	28	1424	2.872
Anterior orbital gyrus L	−20	44	−16	1992	3.205
Temporal pole (superior temporal gyrus) R	38	4	−24	1336	3.201
Temporal pole (superior temporal gyrus) R	32	24	−28	1336	2.810
Precentral gyrus L	−48	−2	24	1152	3.195
Inferior frontal gyrus (triangular part) R	38	16	22	1400	2.981
Rolandic operculum R	48	−2	14	1400	2.608
Temporal pole (superior temporal gyrus) L	−52	18	−16	872	2.899
Temporal pole (superior temporal gyrus) L	−36	20	−28	872	1.758
Fusiform gyrus R	36	−26	−28	1024	2.833
Superior frontal gyrus (medial) L	−10	54	10	696	2.468
Crus I of cerebellar hemisphere R	56	−56	−32	3368	2.408
Inferior temporal gyrus R	70	−44	−16	3368	2.325

difficulties in fear extinction. The preserved stimuli discrimination found in our study, in individuals with high trait anxiety is in line with previous studies involving patients with anxiety (Glotzbach-Schoon et al., 2013). Such studies showed greater differentiation between CS+ and CS− during extinction (Duits et al., 2015; Graner et al., 2020), and showed the same pattern in participants scoring high on rumination (Vanderhasselt et al., 2017). Another factor that might explain higher discrimination between CSs after fear extinction, is the development of a fear response toward the CS− due to its increased ambiguity or uncertainty, particularly in participants scoring high in anxiety questionnaires. For instance, Gazendam et al. (2013), showed that participants with high trait anxiety presented impaired in safety learning, corresponding to higher responses to the CS−. Other studies have explored the association between ambiguity and the tendency to interpret information with a negative cognitive bias. For example, Stuijfzand et al. (2018) showed that negative cognitive bias in face of ambiguity was positively associated with anxiety. It is worth noting that our sample is composed of subclinical-to-healthy participants (with mean STAI 2 [trait] = 39, close to the clinical cutoff (Dibbets & Evers, 2017)), which might explain our results regarding stimuli discrimination. Future studies should implement a fear generalization paradigm and include subjects with both high and low trait anxiety to further clarify how trait anxiety influences both fear extinction, and discrimination/generalization after tDCS.

This study had some limitations that are worth noting. As the study sample comprised solely women, the results cannot be generalized to gender-wise heterogenous populations. This was an intentional methodological choice because women and men are known to differently process (and express) fear-related cues (Day & Stevenson, 2020). Regarding the study design, two limitations should be highlighted and discussed: 1) the quasi-randomized design and 2) the absence of a sham group. On the one hand, the allocation of participants that were not eligible to receive tDCS to the control group, might have contributed to group differences. However, 94% of participants in the control group were randomized (17 out of 18). Nevertheless, results should be interpreted with caution until they are replicated in a fully randomized study. On the other hand, the inclusion of a control group (rather than a sham group), introduced two differences between groups: 1) the actual stimulation, and 2) the expectations of receiving tDCS and associated effects. Therefore, possible placebo effects were not controlled. Current findings warrant replication in a study that includes a third arm (sham group) or a study of two arms fully randomized and placebo controlled. Furthermore, as we only collected behavioral/autonomic fear-related measures on day 1 (arousal, valence, contingency, and SCRs), we could only infer the effect of tDCS modulation based on day 1. Future studies should include other fear extinction measures (such as SCRs and self-reports) pre- and post-tDCS modulation. Finally, it is worth noting that resting-state data was collected before fear extinction, thus informing only about the impact of tDCS over the fear network.

Taken together, cathodal tDCS stimulation over the rdlPFC led to increased neural connectivity during resting-state in fear-processing and emotion regulation regions. Moreover, tDCS has increased fear discrimination between CSs particularly for participants high in trait anxiety, possibly indicating an impaired fear extinction learning. Although our results contribute to a better understanding of the

Table 4 Functional connectivity maps from the left hippocampus in tDCS and control groups. L: left, R: right.

Regions (AAL abbreviation)	MNI coordinates			Clustersize (mm^2)	t−value
	x	y	z		
tDCS group > control group					
Middle frontal gyrus L	−42	50	24	6008	4.100
Rectus L	−14	16	−16	11560	3.232
Medial orbital gyrus R	20	18	−18	11560	2.842
IFG pars orbitalis L	−28	32	−12	11560	2.781
Inferior temporal gyrus L	−40	−8	−34	1616	3.964
Middle frontal gyrus R	38	58	20	3896	3.648
Middle frontal gyrus R	42	42	34	3896	3.020
Middle frontal gyrus R	52	44	14	3896	2.743
Inferior frontal gyrus (triangular part) R	36	30	12	3896	2.711
Superior occipital gyrus R	24	−100	16	1544	3.609
Lobule VIII of cerebellar hemisphere R	18	−72	−44	800	3.524
Fusiform gyrus R	32	−46	−14	1112	3.364
Lobule VI of cerebellar hemisphere R	32	−34	−36	1112	2.125
Insula R	46	6	−6	608	3.357
Lobule VIIB of cerebellar hemisphere L	−10	−78	−46	1024	3.297
Temporal pole (superior temporal gyrus) L	−52	10	−6	1944	3.218
Insula L	−34	16	2	1944	2.260
Insula L	−42	−8	−6	1944	1.989
Middle occipital gyrus L	−28	−88	34	1016	2.967
Middle temporal gyrus L	−42	−56	−4	680	2.631
Temporal pole (superior temporal gyrus) R	54	20	−10	704	2.742
Postcentral gyrus R	52	−32	60	1104	2.732
Crus I of cerebellar hemisphere L	−48	−76	−32	688	2.484
tDCS group < control group					
Precentral gyrus R	14	−18	74	67424	1.777
Precuneus R	2	−58	20	67424	1.796
Angular gyus R	46	−62	32	67424	2.199
Superior frontal gyrus (dorsolateral) R	18	−12	74	67424	6.585
Middle temporal gyrus L	−46	−50	22	67424	5.201
Postcentral gyrus L	−28	−44	58	67424	4.879
Paracentral Lobule L	−4	−18	70	67424	4.753
Precuneus R	2	−48	42	67424	4.616
Middle temporal gyrus L	−64	−28	−14	4048	3.905
Middle temporal gyrus L	−64	−4	−16	4048	3.829
Superior frontal gyrus (medial) R	10	54	30	8576	4.276
Superior frontal gyrus (medial) R	16	50	2	8576	4.102
Supplementary motor area R	12	18	48	8576	3.039
Superior frontal gyrus (dorsolateral) R	16	36	38	8576	2.873
Rectus R	8	48	−18	8576	2.789
Insula L	−28	28	6	856	4.011
Inferior frontal gyrus (triangular part) L	−40	16	22	736	3.909
Superior frontal gyrus (medial) L	−14	50	14	5648	3.853
Superior frontal gyrus (dorsolateral) L	−16	28	42	5648	3.345
Superior frontal gyrus (medial) L	−10	48	40	5648	2.964
Superior frontal gyrus (dorsolateral) L	−12	66	26	5648	2.918
Superior frontal gyrus (dorsolateral) L	−30	58	4	5648	1.951
Middle occipital gyrus L	−36	−68	24	4664	3.830
Inferior occipital gyrus L	−40	−82	−4	4664	2.959
Inferior parietal gyrus L	−34	−72	46	4664	2.580
Lingual gyrus L	−6	−74	−8	2624	3.562
Lingual gyrus R	10	−86	−6	2624	3.186
Inferior occipital gyrus R	24	−102	−12	2624	2.156
Lobule III of cerebellar hemisphere R	14	−34	−14	1592	3.557
SupraMarginal gyrus R	44	−34	26	576	3.523
Middle frontal gyrus R	34	44	−12	856	3.474
Fusiform gyrus R	40	−24	−30	6288	3.423

Table 4 (*Continued*)

Regions (AAL abbreviation)	MNI coordinates			Clustersize (mm^2)	t−value
	x	y	z		
Middle temporal gyrus R	58	−20	−16	6288	3.254
Middle temporal gyrus R	64	−2	−28	6288	3.236
Temporal pole (middle temporal gyrus) R	34	24	−36	6288	3.154
Temporal pole (middle temporal gyrus) R	52	14	−40	6288	2.665
Superior parietal gyrus R	20	−50	70	792	3.381
Precentral gyrus R	52	0	28	656	3.348
Middle frontal gyrus R	38	24	42	1176	3.267
Anterior cingulate cortex (subgenual) L	−6	28	−8	664	3.222
Rectus R	10	26	−22	1272	2.374
Lobule VIII of cerebellar hemisphere R	16	−64	−54	960	2.109
Inferior frontal gyrus (triangular part) L	−56	20	8	752	2.650
Precentral gyrus R	60	−8	48	576	2.545

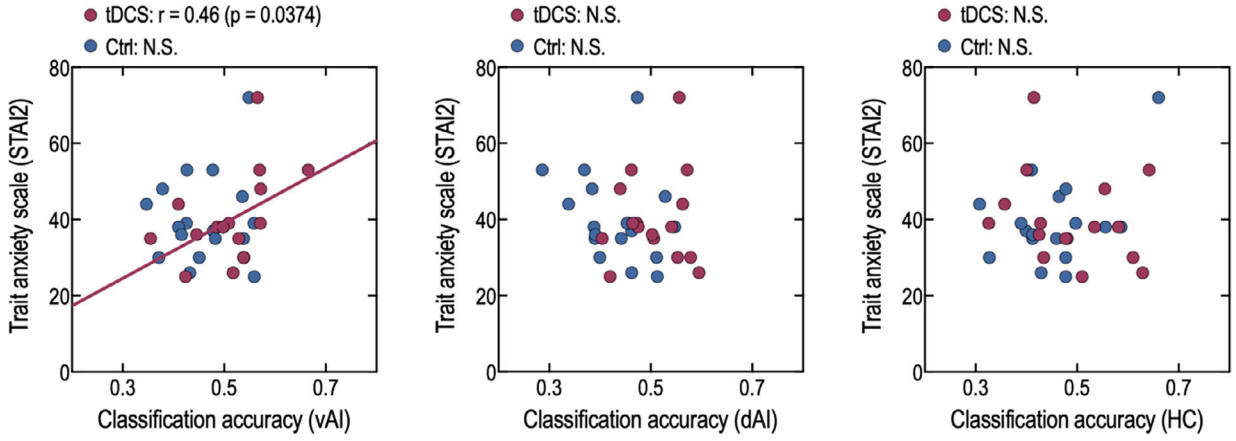

Fig. 4 Results of correlation analysis between the classification accuracy and state-state anxiety inventory in the left vAI (A), dAI (B), and HC.

neural mechanisms underlying tDCS effect, its impact on fear extinction processes and clinical symptoms improvement warrants further studies to be clarified.

Funding

AGA was supported by the Foundation for Science and Technology, Portugal and Programa COMPETE [grants numbers SFRH/BD/80945/2011, PTDC/MHC-PAP/5618/2014 (POCI-01-0145FEDER-016836); http://www.poci-compete2020.pt/]. DL was supported by the KBRI basic research program through Korea Brain Research Institute funded by Ministry of Science and ICT (22-BR-05-02, 22-BR-04-03) and the National Research Foundation of Korea (NRF) grant funded by the Korea government (MSIT) (NRF-2021R1F1A1062514). RG was supported by a Ph.D. Grant (SFRH/BD/5099/2020), sponsored by FCT (Portuguese Foundation for Science and Technology). JA was supported by the European Research Council (Starting Grant number 802553 "ContentMAP").

Author contributions

DL: Formal analysis, Funding acquisition, Visualization, Writing – original draft, Writing – review & editing. **RG:** Data curation, Data acquisition, Investigation, Writing – original draft, review & editing. **ÓFG:** Writing – review & editing. **JA:** Writing – review & editing. **AGA:** Conceptualization, Formal analysis, Funding acquisition, Supervision, Writing – original draft, Writing – review & editing.

Conflict of Interest

The authors declare that the research was conducted in the absence of any commercial or financial relationships that could be construed as a potential conflict of interest.

References

Abend, R., Jalon, I., Gurevitch, G., Sar-El, R., Shechner, T., Pine, D. S., Hendler, T., & Bar-Haim, Y. (2016). Modulation of fear extinction processes using transcranial electrical stimulation. *Translational Psychiatry*, *6*(10), e913. https://doi.org/10.1038/tp.2016.197.

Agren, T., Engman, J., Frick, A., Björkstrand, J., Larsson, E. M., Furmark, T., & Fredrikson, M. (2012). Disruption of reconsolidation erases a fear memory trace in the human amygdala. *Science*, *337*(6101), 1550–1552. https://doi.org/10.1126/science.

Andersson, P., Pluim, J. P., Viergever, M. A., & Ramsey, N. F. (2013). Navigation of a telepresence robot via covert visuospatial

attention and real-time fMRI. *Brain Topography*, *26*(1), 177–185. https://doi.org/10.1007/s10548-012-0252-z.

Antal, A., Bikson, M., Datta, A., Lafon, B., Dechent, P., Parra, L. C., & Paulus, W. (2014). Imaging artifacts induced by electrical stimulation during conventional fMRI of the brain. *Neuroimage*, *85*(Pt 3), 1040–1047. https://doi.org/10.1016/j.neuroimage.2012.10.026.

Berntson, G. G., Norman, G. J., Bechara, A., Bruss, J., Tranel, D., & Cacioppo, J. T. (2011). The insula and evaluative processes. *Psychological Science*, *22*(1), 80–86. https://doi.org/10.1177/0956797610391097.

Boser, B. E., & Guyon, I. (1992). A training algorithm for optimal margin classifiers. In *Proceedings of the fifth annual workshop on computational learning theory* (pp. 144—152).

Boucsein, W., Fowles, D. C., Grimnes, S., Ben-Shakhar, G., roth, W. T., Dawson, M. E., Filion, D. L., & Society for Psychophysiological Research Ad Hoc Committee on Electrodermal, M. (2012). Publication recommendations for electrodermal measurements. *Psychophysiology*, 49(8), 1017-1034.https://doi.org/10.1111/j.1469-8986.2012.01384.x.

Bradley, R., Greene, J., Russ, E., Dutra, L., & Westen, D. (2005). A multidimensional meta-analysis of psychotherapy for PTSD. *American Journal of Psychiatry*, *162*(2), 214–227. https://doi.org/10.1176/appi.ajp.162.2.214.

Bullmore, E., & Sporns, O. (2009). Complex brain networks: graph theoretical analysis of structural and functional systems. *Nature Reviews Neuroscience*, *10*(3), 186–198. https://doi.org/10.1038/nrn2575.

Chen, Q., Garcea, F. E., & Mahon, B. Z. (2016). The representation of object-directed action and function knowledge in the human brain. *Cerebral Cortex*, *26*(4), 1609–1618. https://doi.org/10.1093/cercor/bhu328.

Clarke, P. J. F., Sprlyan, B. F., Hirsch, C. R., Meeten, F., & Notebaert, L. (2020). tDCS increases anxiety reactivity to intentional worry. *Journal of Psychiatric Research*, *120*, 34–39. https://doi.org/10.1016/j.jpsychires.2019.10.013.

Cortes, C., & Vapnik, V. (1995). Support-vector network. *Machine Learning*, *20*, 273–297.

Day, H. L. L., & Stevenson, C. W. (2020). The neurobiological basis of sex differences in learned fear and its inhibition. *European Journal of Neuroscience*, *52*(1), 2466–2486. https://doi.org/10.1111/ejn.14602.

Deco, G., Jirsa, V. K., & McIntosh, A. R. (2011). Emerging concepts for the dynamical organization of resting-state activity in the brain. *Nature Reviews Neuroscience*, *12*(1), 43–56. https://doi.org/10.1038/nrn2961.

Deco, G., Tononi, G., Boly, M., & Kringelbach, M. L. (2015). Rethinking segregation and integration: contributions of whole-brain modelling. *Nature Reviews Neuroscience*, *16*(7), 430–439. https://doi.org/10.1038/nrn3963.

Dibbets, P., & Evers, E. A. (2017). The influence of state anxiety on fear discrimination and extinction in females. *Frontiers in Psychology*, *8*, 347. https://doi.org/10.3389/fpsyg.2017.00347.

Diekhof, E. K., Geier, K., Falkai, P., & Gruber, O. (2011). Fear is only as deep as the mind allows: a coordinate-based meta-analysis of neuroimaging studies on the regulation of negative affect. *Neuroimage*, *58*(1), 275–285. https://doi.org/10.1016/j.neuroimage.2011.05.073.

Dittert, N., Huttner, S., Polak, T., & Herrmann, M. J. (2018). Augmentation of fear extinction by transcranial direct current stimulation (tDCS). *Frontiers in Behavioral Neuroscience*, *12*, 76. https://doi.org/10.3389/fnbeh.2018.00076.

Duits, P., Cath, D. C., Lissek, S., Hox, J. J., Hamm, A. O., Engelhard, I. M., van den Hout, M. A., & Baas, J. M. (2015). Updated meta-analysis of classical fear conditioning in the anxiety disorders. *Depression and Anxiety*, *32*(4), 239–253. https://doi.org/10.1002/da.22353.

Dunsmoor, J. E., Kroes, M. C. W., Li, J., Daw, N. D., Simpson, H. B., & Phelps, E. A. (2019). Role of human ventromedial prefrontal cortex in learning and recall of enhanced extinction. *Journal of Neuroscience*, *39*(17), 3264–3276. https://doi.org/10.1523/JNEUROSCI.2713-18.2019.

Eysenck, H. J. (1979). The conditioning model of neurosis. *Behavioral and Brain Sciences*, *2*, 155–199.

Fitzgerald, P. J., Seemann, J. R., & Maren, S. (2014). Can fear extinction be enhanced? A review of pharmacological and behavioral findings. *Brain Research Bulletin*, 105, 46-60. https://doi.org/10.1016/j.brainresbull.2013.12.007

Foa, E. B., & McLean, C. P. (2016). The efficacy of exposure therapy for anxiety-related disorders and its underlying mechanisms: The case of OCD and PTSD. *Annual Review of Clinical Psychology*, *12*, 1-28. https://doi.org/10.1146/annurev-clinpsy-021815-093533.

Friston, K., Holmes, A., Worsley, K., Poline, J., Frith, C., & Frackowiak, R. (1995). Statistical parametric maps in functional imaging: a general linear approach. *Human Brain Mapping*, *2*, 189–210.

Friston, K. J. (2011). Functional and effective connectivity: A review. *Brain Connect*, *1*(1), 13–36. https://doi.org/10.1089/brain.2011.0008.

Frontera, J. L., Baba Aissa, H., Sala, R. W., Mailhes-Hamon, C., Georgescu, I. A., Lena, C., & Popa, D. (2020). Bidirectional control of fear memories by cerebellar neurons projecting to the ventrolateral periaqueductal grey. *Nature Communication*, *11*(1), 5207. https://doi.org/10.1038/s41467-020-18953-0.

Fullana, M. A., Albajes-Eizagirre, A., Soriano-Mas, C., Vervliet, B., Cardoner, N., Benet, O., Radua, J., & Harrison, B. J. (2018). Fear extinction in the human brain: A meta-analysis of fMRI studies in healthy participants. *Neuroscience and Biobehavioral Reviews*, *88*, 16–25. https://doi.org/10.1016/j.neubiorev.2018.03.002.

Fullana, M. A., Harrison, B. J., Soriano-Mas, C., Vervliet, B., Cardoner, N., Avila-Parcet, A., & Radua, J. (2016). Neural signatures of human fear conditioning: an updated and extended meta-analysis of fMRI studies. *Molecular Psychiatry*, *21*(4), 500–508. https://doi.org/10.1038/mp.2015.88.

Ganho-Avila, A., Goncalves, O. F., Guiomar, R., Boggio, P. S., Asthana, M. K., Krypotos, A. M., & Almeida, J. (2019). The effect of cathodal tDCS on fear extinction: A cross-measures study. *Plos One*, *14*,(9) e0221282. https://doi.org/10.1371/journal.pone.0221282.

Ganho-Ávila, A., Guiomar, R., Valério, D., Gonçalves, Ó. F., & Almeida, J (2022). Offline tDCS modulates prefrontal-cortical-subcortical-cerebellar fear pathways in delayed fear extinction. *Experimental Brain Research*, *240*(1), 221–235. https://doi.org/10.1007/s00221-021-06248-9.

Ganho-Avila, A., Guiomar, R., Valerio, D., Goncalves, O. F., & Almeida, J. (2022). Offline tDCS modulates prefrontal-cortical-subcortical-cerebellar fear pathways in delayed fear extinction. *Experimental Brain Research*, *240*(1), 221–235. https://doi.org/10.1007/s00221-021-06248-9.

Ganho-Ávila, A., Goncalves, O. F., Guiomar, R., Boggio, P. S., Asthana, M. K., Krypotos, A. M., & Almeida, J. (2019). The effect of cathodal tDCS on fear extinction: A cross-measures study. *PLoS One*, *14*(9), e0221282. https://doi.org/10.1371/journal.pone.0221282.

Gazendam, F. J., Kamphuis, J. H., & Kindt, M. (2013). Deficient safety learning characterizes high trait anxious individuals. *Biological Psychology*, *92*(2), 342–352. https://doi.org/10.1016/j.biopsycho.2012.11.006.

Gilmartin, M. R., Balderston, N. L., & Helmstetter, F. J. (2014). Prefrontal cortical regulation of fear learning. *Trends in Neuroscience (Tins)*, *37*(8), 455–464. https://doi.org/10.1016/j.tins.2014.05.004.

Glotzbach-Schoon, E., Tadda, R., Andreatta, M., Troger, C., Ewald, H., Grillon, C., Pauli, P., & Muhlberger, A. (2013). Enhanced discrimination between threatening and safe contexts

in high-anxious individuals. *Biological Psychology*, *93*(1), 159–166. https://doi.org/10.1016/j.biopsycho.2013.01.011.

Graner, J. L., Stjepanovic, D., & LaBar, K. S. (2020). Extinction learning alters the neural representation of conditioned fear. *Cogn Affect Behav Neurosci*, *20*(5), 983–997. https://doi.org/10.3758/s13415-020-00814-4.

Gu, X., Hof, P. R., Friston, K. J., & Fan, J. (2013). Anterior insular cortex and emotional awareness. *Journal of Comparative Neurology*, *521*(15), 3371–3388. https://doi.org/10.1002/cne.23368.

Hauner, K. K., Mineka, S., Voss, J. L., & Paller, K. A. (2012). Exposure therapy triggers lasting reorganization of neural fear processing. *PNAS*, *109*(23), 9203–9208. https://doi.org/10.1073/pnas.1205242109.

Haxby, J. V., Gobbini, M. I., Furey, M. L., Ishai, A., Schouten, J. L., & Pietrini, P. (2001). Distributed and overlapping representations of faces and objects in ventral temporal cortex. *Science*, *293*(5539), 2425–2430. https://doi.org/10.1126/science.1063736.

Haynes, J. D., & Rees, G. (2006). Decoding mental states from brain activity in humans. *Nature Reviews Neuroscience*, *7*(7), 523–534. https://doi.org/10.1038/nrn1931.

Herry, C., Ferraguti, F., Singewald, N., Letzkus, J. J., Ehrlich, I., & Luthi, A. (2010). Neuronal circuits of fear extinction. *European Journal of Neuroscience*, *31*(4), 599–612. https://doi.org/10.1111/j.1460-9568.2010.07101.x.

Huskisson, E. C. (1974). Measurement of pain. *Lancet*, *2*(7889), 1127–1131. https://doi.org/10.1016/s0140-6736(74)90884-8.

Ironside, M., Browning, M., Ansari, T. L., Harvey, C. J., Sekyi-Djan, M. N., Bishop, S. J., Harmer, C. J., & O'Shea, J (2019). Effect of prefrontal cortex stimulation on regulation of amygdala response to threat in individuals with trait anxiety: A randomized clinical trial. *JAMA Psychiatry*, *76*(1), 71–78. https://doi.org/10.1001/jamapsychiatry.2018.2172.

Kamitani, Y., & Tong, F. (2005). Decoding the visual and subjective contents of the human brain. *Nature Neuroscience*, *8*(5), 679–685. https://doi.org/10.1038/nn1444.

Klem, G. H., Lüders, H. O., Jasper, H. H., & Elger, C. (1999). The ten-twenty electrode system of the International Federation. The International Federation of Clinical Neurophysiology. *Electroencephalography and Clinical Neurophysiology Supplement*, *52*, 3–6.

Kriegeskorte, N., Goebel, R., & Bandettini, P. (2006). Information-based functional brain mapping. *PNAS*, *103*(10), 3863–3868. https://doi.org/10.1073/pnas.0600244103.

LaBar KS, G. J., Gore, JC, LeDoux, JE, & Phelps, EA (1998). Human amygdala activation during conditioned fear acquisition and extinction: A mixed-trial fMRI study. *Neuron*, *20*(5), 937–945. https://doi.org/10.1016/s0896-6273(00)80475-4.

LeDoux, J. E., & Phelps, E. A. (2008). *Emotional networks in the brain*.

Lee, D., Mahon, B. Z., & Almeida, J. (2019). Action at a distance on object-related ventral temporal representations. *Cortex; A Journal Devoted to the Study of the Nervous System and Behavior*, *117*, 157–167. https://doi.org/10.1016/j.cortex.2019.02.018.

Lonsdorf, T. B., Menz, M. M., Andreatta, M., Fullana, M. A., Golkar, A., Haaker, J., Heitland, I., Hermann, A., Kuhn, M., Kruse, O., Meir Drexler, S., Meulders, A., Nees, F., Pittig, A., Richter, J., Romer, S., Shiban, Y., Schmitz, A., Straube, B., … Merz, C. J. (2017). Don't fear 'fear conditioning': Methodological considerations for the design and analysis of studies on human fear acquisition, extinction, and return of fear. *Neuroscience and Biobehavioral Reviews*, *77*, 247–285. https://doi.org/10.1016/j.neubiorev.2017.02.026.

Marin, M. F., Camprodon, J. A., Dougherty, D. D., & Milad, M. R. (2014). Device-based brain stimulation to augment fear extinction: implications for PTSD treatment and beyond. *Depression and Anxiety*, *31*(4), 269–278. https://doi.org/10.1002/da.22252.

Milad, M. R., Wright, C. I., Orr, S. P., Pitman, R. K., Quirk, G. J., & Rauch, S. L. (2007). Recall of fear extinction in humans activates the ventromedial prefrontal cortex and hippocampus in concert. *Biological Psychiatry*, *62*(5), 446–454. https://doi.org/10.1016/j.biopsych.2006.10.011.

Nitsche, M. A., & Paulus, W. (2000). Excitability changes induced in the human motor cortex by weak transcranial direct current stimulation. *Journal of Physiology*, *527*(Pt 3), 633–639. https://doi.org/10.1111/j.1469-7793.2000.t01-1-00633.x.

Norman, K. A., Polyn, S. M., Detre, G. J., & Haxby, J. V. (2006). Beyond mind-reading: multi-voxel pattern analysis of fMRI data. *Trends in Cognitive Sciences*, *10*(9), 424–430. https://doi.org/10.1016/j.tics.2006.07.005.

Oyarzun, J. P., Lopez-Barroso, D., Fuentemilla, L., Cucurell, D., Pedraza, C., Rodriguez-Fornells, A., & de Diego-Balaguer, R. (2012). Updating fearful memories with extinction training during reconsolidation: a human study using auditory aversive stimuli. *Plos One*, *7*(6), e38849. https://doi.org/10.1371/journal.pone.0038849.

Park, H. J., & Friston, K. (2013). Structural and functional brain networks: from connections to cognition. *Science*, *342*,(6158) 1238411. https://doi.org/10.1126/science.1238411.

Pereira, F., Mitchell, T., & Botvinick, M. (2009). Machine learning classifiers and fMRI: a tutorial overview. *Neuroimage*, *45*(1 Suppl), S199–S209. https://doi.org/10.1016/j.neuroimage.2008.11.007.

Phelps, E. A., Delgado, M. R., Nearing, K. I., & LeDoux, J. E. (2004). Extinction learning in humans: role of the amygdala and vmPFC. *Neuron*, *43*(6), 897–905. https://doi.org/10.1016/j.neuron.2004.08.042.

Pitman, R. K., & Orr, S. P. (1986). Test of the conditioning model of neurosis: differential aversive conditioning of angry and neutral facial expressions in anxiety disorder patients. *Journal of Abnormal Psychology*, *95*(3), 208–213. https://doi.org/10.1037//0021-843x.95.3.208.

Quirk, G. J., & Mueller, D. (2008). Neural mechanisms of extinction learning and retrieval. *Neuropsychopharmacology*, *33*(1), 56–72. https://doi.org/10.1038/sj.npp.1301555.

Repa, J. C., Muller, J., Apergis, J., Desrochers, T. M., Zhou, Y., & LeDoux, J. E. (2001). Two different lateral amygdala cell populations contribute to the initiation and storage of memory. *Nature Neuroscience*, *4*(7), 724–731. https://doi.org/10.1038/89512.

Sadeghi Movahed, F., Alizadeh Goradel, J., Pouresmali, A., & Mowlaie, M. (2018). Effectiveness of transcranial direct current stimulation on worry, anxiety, and depression in generalized anxiety disorder: a randomized, single-blind pharmacotherapy and sham-controlled clinical trial. *Iranian Journal of Psychiatry and Behavioral Sciences*, *12*(2).

Scholz, J., Klein, M. C., Behrens, T. E., & Johansen-Berg, H. (2009). Training induces changes in white-matter architecture. *Nature Neuroscience*, *12*(11), 1370–1371. https://doi.org/10.1038/nn.2412.

Schwarzbach, J. (2011). A simple framework (ASF) for behavioral and neuroimaging experiments based on the psychophysics toolbox for MATLAB. *Behav Res Methods*, *43*(4), 1194–1201. https://doi.org/10.3758/s13428-011-0106-8.

Sevenster, D., Visser, R. M., & D'Hooge, R (2018). A translational perspective on neural circuits of fear extinction: Current promises and challenges. *Neurobiology of Learning and Memory*, *155*, 113–126. https://doi.org/10.1016/j.nlm.2018.07.002.

Shiozawa, P., Leiva, A. P., Castro, C. D., da Silva, M. E., Cordeiro, Q., Fregni, F., & Brunoni, A. R. (2014). Transcranial direct current stimulation for generalized anxiety disorder: a case study. *Biological Psychiatry*, *75*(11), e17–e18. https://doi.org/10.1016/j.biopsych.2013.07.014.

Sitaram, R., Lee, S., Ruiz, S., Rana, M., Veit, R., & Birbaumer, N. (2011). Real-time support vector classification and feedback of multiple emotional brain states. *Neuroimage*, *56*(2), 753–765. https://doi.org/10.1016/j.neuroimage.2010.08.007.

Sjouwerman, R., Scharfenort, R., & Lonsdorf, T. B. (2020). Individual differences in fear acquisition: multivariate analyses of

different emotional negativity scales, physiological responding, subjective measures, and neural activation. *Science Reports*, 10 (1), 15283. https://doi.org/10.1038/s41598-020-72007-5.

Sotres-Bayon, F., Cain, C. K., & LeDoux, J. E. (2006). Brain mechanisms of fear extinction: historical perspectives on the contribution of prefrontal cortex. *Biological Psychiatry*, *60*(4), 329–336. https://doi.org/10.1016/j.biopsych.2005.10.012.

Spielberger, C. D. (1983). *Manual for the state-trait anxiety inventory STAI (form Y) ("self-evaluation questionnaire").*

Stein, D. J., Fernandes Medeiros, L., Caumo, W., & Torres, I. L. (2020). Transcranial direct current stimulation in patients with anxiety: Current perspectives. *Neuropsychiatric Disease and Treatment*, *16*, 161–169. https://doi.org/10.2147/NDT.S195840.

Stuijfzand, S., Creswell, C., Field, A. P., Pearcey, S., & Dodd, H. (2018). Research Review: Is anxiety associated with negative interpretations of ambiguity in children and adolescents? A systematic review and meta-analysis. *Journal of Child Psychology and Psychiatry and Allied Disciplines*, *59*(11), 1127-1142. https://doi.org/10.1111/jcpp.12822.

Thair, H., Holloway, A. L., Newport, R., & Smith, A. D. (2017). Transcranial Direct Current Stimulation (tDCS): A beginner's guide for design and implementation. *Frontiers in Neuroscience*, (641), 11. https://doi.org/10.3389/fnins.2017.00641.

Todd, M. T., Nystrom, L. E., & Cohen, J. D. (2013). Confounds in multivariate pattern analysis: Theory and rule representation case study. *Neuroimage*, *77*, 157–165. https://doi.org/10.1016/j.neuroimage.2013.03.039.

van 't Wout, M., Mariano, T. Y., Garnaat, S. L., Reddy, M. K., Rasmussen, S. A., & Greenberg, B. D. (2016). Can transcranial direct current stimulation augment extinction of conditioned fear? *Brain Stimulation*, *9*(4), 529–536. https://doi.org/10.1016/j.brs.2016.03.004.

Vanderhasselt, M. A., Sanchez, A., Josephy, H., Baeken, C., Brunoni, A. R., & De Raedt, R. (2017). Anodal tDCS over the right dorsolateral prefrontal cortex modulates cognitive processing of emotional information as a function of trait rumination in healthy volunteers. *Biological Psychology*, *123*, 111–118. https://doi.org/10.1016/j.biopsycho.2016.12.006.

Ward, B. D. (2000). Simultaneous inference for fMRI data. https://doi.org/https://afni.nimh.nih.gov/pub/dist/doc/manuals/AlphaSim.pdf.

Whitehead, J. C., & Armony, J. L. (2019). Multivariate fMRI pattern analysis of fear perception across modalities. *European Journal of Neuroscience*, *49*(12), 1552–1563. https://doi.org/10.1111/ejn.14322.

Xiong, J., Gao, J. H., Lancaster, J. L., & Fox, P. T. (1995). Clustered pixels analysis for functional MRI activation studies of the human brain. *Human Brain Mapping*, *3*, 287–301.

Yang, W., Makita, K., Nakao, T., Kanayama, N., Machizawa, M. G., Sasaoka, T., Sugata, A., Kobayashi, R., Hiramoto, R., Yamawaki, S., Iwanaga, M., & Miyatani, M. (2018). Affective auditory stimulus database: An expanded version of the International Affective Digitized Sounds (IADS-E). *Behavior Research Methods*, *50*(4), 1415–1429. https://doi.org/10.3758/s13428-018-1027-6.

Zhou, F., Zhao, W., Qi, Z., Geng, Y., Yao, S., Kendrick, K. M., Wager, T. D., & Becker, B. (2021). A distributed fMRI-based signature for the subjective experience of fear. *Nature Communication*, *12*(1), 6643. https://doi.org/10.1038/s41467-021-26977-3.